American Mineralogist, Volume 98, pages 1930–1937, 2013

AMORPHOUS MATERIALS: PROPERTIES, STRUCTURE, AND DURABILITY

North American microtektites are more oxidized than tektites†

GABRIELE GIULI[1,*], MARIA RITA CICCONI[1], SIGRID GRIET EECKHOUT[2,‡], CHRISTIAN KOEBERL[3], BILLY P. GLASS[4], GIOVANNI PRATESI[5], MARIANGELA CESTELLI-GUIDI[6] AND ELEONORA PARIS[1]

[1]School of Science and Technology, Geology Division, University of Camerino, Via Gentile III da Varano, 62032, Italy
[2]European Synchrotron Radiation Facility (ESRF), 6 rue Jules Horowitz, 38043 Grenoble, France
[3]Department of Lithospheric Research, University of Vienna, Althanstrasse 14, A-1090 Vienna, Austria; *and* Natural History Museum, Burgring 7, A-1010 Vienna, Austria
[4]Department of Geological Sciences, University of Delaware, Newark, Delaware 19716, U.S.A.
[5]Dipartimento di Scienze della Terra, Università di Firenze, Via G. La Pira 4, 50121, Firenze, Italy
[6]Laboratori Nazionali Frascati, Istituto Nazionale Fisica Nucleare, Via Enrico Fermi, Frascati, Italy

ABSTRACT

Iron oxidation states and coordination numbers have been determined by micro-X-ray absorption near edge spectroscopy (XANES) on the cores of a large group of microtektites from the Australasian, Ivory Coast, and North American (NA) tektite strewn field. The North American microtektites used in this study have been collected from five sites at different distances from the source crater; most have SiO_2 content between 70 and 80 wt%. Accurate analysis of the pre-edge peak energy position and integrated area allowed determination of $Fe^{3+}/(Fe^{2+}+Fe^{3+})$ ratios on all samples with an estimated error of ±0.05.

Microtektites from the Australasian and Ivory Coast strewn fields show low values of the $Fe^{3+}/(Fe^{2+}+Fe^{3+})$ ratios, in fair agreement with tektites from the same strewn field. In contrast, microtektites from the North American strewn fields show a wide range of $Fe^{3+}/(Fe^{2+}+Fe^{3+})$ ratios from 0.02 to ca. 0.61. Comparison of Fe oxidation state data with chemical composition do not show any relation between $Fe^{3+}/(Fe^{2+}+Fe^{3+})$ ratios and Na, Ca, or K contents, thus suggesting that the high-Fe oxidation states are not the consequence of sea-water alteration.

The difference between the Fe oxidation state of tektites and microtektites from the North American strewn fields suggests that some factors in the formation of the North American microtektites were different than for the North American tektites and for microtektites in the other strewn fields.

Previous Fe oxidation state data on NA tektites strongly suggest that the wide range in Fe oxidation state we found on NA microtektites is not related to lateral heterogeneity of the target rocks. Despite a correlation between microtektite oxidation state and distance from the source crater, we maintain that Fe oxidation state is not related only to the microtektite droplet flight distance. This is in keeping with the fact that no significant variations in the Fe oxidation state have been found in microtektites from the Australasian strewn field, even for Australasian microtektites recovered in Antarctica. The Fe oxidation state in North American microtektites could be explained by interaction of melt droplets with a H_2O-rich vapor plumes generated during the impact. These data point out that some difference must exist between the thermal histories of microtektites and tektites from the NA strewn field. Moreover, microtektites from the NA strewn field show also distinctively higher oxidation states than those from Ivory Coast or the Australasian strewn fields.

Keywords: Impact glasses, tektites, microtektites, Fe local structure, XANES

INTRODUCTION

Microtektites are small (<1 mm) splash-form impact glasses related to tektites, which are found scattered over regions of the Earth's surface called strewn fields (e.g., Koeberl 1986, 1994). They are associated with three of the four tektite strewn fields so far known: the North American (NA), the Ivory Coast, and the Australasian strewn fields. They are generally found in deep-sea cores (e.g., Glass 1967, 1968, 1972; Cassidy et al. 1969), and their distribution greatly contributed to establish the limits of tektites strewn fields (see Glass 1990; Glass and Pizzuto 1994).

Despite the availability of geochemical studies on microtektites (see Glass et al. 2004 and references therein), few studies exist of the Fe coordination number and oxidation state in such materials (Senftle et al. 1969). As microtektites constitute a large fraction of the mass of glass produced by a tektite-generating impact event, such studies are of great importance for a more

* E-mail: gabriele.giuli@unicam.it
‡ Present address: ONDRAS NIRAS, avenue des Arts 14, Bruxelles, 1210, Belgium.

† Special Collection: Amorphous Materials: Properties, Structure, and Durability. Special associate editors Daniel Neuville and Grant Henderson. Information about the Amorphous Materials special collection papers can be found on GSW at http://ammin.geoscienceworld.org/site/misc/specialissuelist.xhtml. Additionally the GSW site has a classification tag found on the right-hand side of the article that is a link to all these papers. The MSA website (http://www.minsocam.org/MSA/AmMin/AmMineral.html) has complete information.

0003-004X/13/1112–1930$05.00/DOI: http://dx.doi.org/10.2138/am.2013.4505

TABLE 1. Composition of the studied microtektites in wt% oxides

Sample	core	SiO_2	Al_2O_3	Cr_2O_3	FeO	CaO	MgO	K_2O	Na_2O	TiO_2	Total	Source
Australasian microtektites												
805-1	ODP769A	64.72	16.21	0.03	5.39	3.9	7.77	0.48	0.62	0.87	99.99	1
805-2	ODP769A	70.09	13.54	0.01	5.74	2.68	3.02	2.77	1.37	0.75	99.97	1
805-3	ODP769A	66.84	16.71	0.01	5.65	2.72	2.62	3.21	1.39	0.83	99.98	1
805-4	RC12-331	56.05	20.66	0.05	4.5	5.72	11.34	0.13	0.43	1.17	100.05	1
805-5	RC14-46	67.17	14.94	0.01	5.97	3.68	3.07	2.79	1.59	0.8	100.02	1
805-6	RC14-46	69.25	12.48	0.04	6.77	3.29	4.17	2.22	1.04	0.69	99.95	1
Ivory Coast microtektites												
858-1	K9-56	63.68	17.62	0.05	7.44	2.09	6.15	1.03	1.67	0.57	100.30	1
858-2	K9-56	69.30	15.82	0.02	5.67	1.48	3.25	1.89	2.10	0.47	100.00	1
858-3	K9-56	67.35	17.15	0.01	6.39	1.56	3.13	1.90	1.98	0.54	100.01	1
858-4	K9-56	67.33	16.50	0.02	6.48	1.63	3.86	1.65	1.96	0.58	100.01	1
858-5	K9-56	67.12	15.97	0.02	6.53	1.88	4.20	1.82	1.96	0.50	100.00	1
858-6	K9-56	67.38	16.89	0.02	6.31	1.54	3.31	1.96	2.09	0.52	100.02	1
858-7	K9-56	68.11	17.02	0.02	6.67	1.05	2.91	2.03	1.60	0.54	99.95	1
858-8	K9-56	67.86	16.23	0.02	6.34	1.81	3.84	1.54	1.80	0.53	99.97	1
858-9	K9-56	68.00	16.90	0.02	6.55	1.14	3.15	1.95	1.72	0.58	100.01	1
858-10	K9-56	67.59	16.73	0.02	6.19	1.54	3.37	1.96	2.03	0.54	99.97	1
North American microtektites												
772-1	DSDP94	71.44	17.62	0.05	5.98	0.43	0.95	1.64	1.05	0.90	100.06	1
772-2	DSDP94	77.87	11.66	0.02	3.09	1.29	1.10	3.16	1.22	0.60	100.01	1
772-3	DSDP94	74.36	13.82	0.03	3.51	2.01	1.68	2.60	1.25	0.74	100.00	1
772-4	DSDP94	78.47	11.78	0.02	3.12	1.30	1.23	2.52	0.94	0.60	99.98	1
772-5	DSDP94	73.60	13.87	0.05	4.17	1.78	1.76	2.74	1.32	0.76	100.05	1
772-6	DSDP94	81.51	10.82	0.01	2.28	0.45	0.80	2.74	0.92	0.46	99.99	1
772-7	DSDP94	79.97	11.03	0.02	2.78	0.94	0.96	3.02	0.78	0.51	100.01	1
392-1	DSDP612	71.01	16.10	n.d.	4.16	1.61	1.23	1.40	3.01	0.85	99.37	3
392-2	DSDP612	67.38	15.50	n.d.	5.43	2.63	3.49	1.52	2.65	0.75	99.35	2
392-6	DSDP612	69.94	15.10	n.d.	4.33	2.11	2.60	1.51	3.19	0.65	99.43	2
151-91a	RC9-58	75.19	12.73	n.d.	3.04	1.52	1.30	4.07	1.28	0.46	99.59	3
151-93b	RC9-58	67.52	16.06	n.d.	5.51	1.42	1.69	4.84	1.45	1.07	99.56	3
151-94a	RC9-58	79.63	11.31	n.d.	2.59	0.52	1.00	2.95	1.02	0.53	99.55	3
151-102a	RC9-58	76.12	13.37	n.d.	3.62	0.97	1.00	2.99	0.92	0.66	99.65	3
775-1	DSDP149	71.38	14.57	n.d.	4.29	1.55	1.95	4.30	1.24	0.73	100.01	1
775-2	DSDP149	72.22	15.63	n.d.	4.90	1.15	1.48	2.86	0.89	0.85	99.98	1
775-3	DSDP149	70.72	16.30	n.d.	4.68	1.56	1.68	3.20	1.01	0.84	99.99	1
312-2	Barbados	75.40	13.20	n.d.	4.95	0.76	1.00	2.31	0.92	0.60	99.14	4
312-3	Barbados	75.40	13.60	n.d.	3.58	1.26	0.97	2.70	1.02	0.65	99.18	4
312-4	Barbados	78.90	13.70	n.d.	1.56	1.88	0.70	1.55	0.21	0.61	99.11	4
312-5	Barbados	77.80	12.40	n.d.	2.78	1.03	0.64	3.08	0.98	0.52	99.23	4
312-6	Barbados	76.10	13.30	n.d.	3.75	0.77	0.69	2.33	1.59	0.69	99.22	4
312-7	Barbados	73.80	14.20	n.d.	4.29	1.43	1.17	2.65	1.32	0.68	99.54	4

Note: 1 = Glass et al. (2004); 2 = Glass (1989); 3 = this study; 4 = Burns (1985).

complete understanding of impact-generated glasses and, in particular, to try reconstructing the oxygen fugacity conditions prevailing during impact melt formation.

Previous data have shown a set of microtektites from the North American strewn field (collected at the DSDP Site 94) to be consistently more oxidized with respect to microtektites from the other strewn fields (Giuli et al. 2008b). Moreover, another study of macroscopic tektites from the North American strewn fields showed no variation of the Fe oxidation state as a function of tektite provenance and composition (Giuli et al. 2010a), thus confirming that the strong variation in the Fe oxidation state previously found in NA microtektites does not depend on lateral heterogeneities of the target rock.

This case is unique among tektites and microtektites and, if confirmed, may contribute to a better understanding of microtektite formation processes. To expand on our previous data, we studied a larger set of microtektites from the North American strewn field collected from three additional cores (RC9-58 and DSDP sites 612 and 149) and from Barbados. These samples have been collected at different distances from the source crater and span a wider compositional range than those previously analyzed. The use of a small X-ray beam allowed to probe the core of the studied samples, thus avoiding possible alteration rims.

SAMPLES AND EXPERIMENTAL

Microtektite samples consist of glassy spherules retrieved from deep-sea cores from three different strewn fields: Australasian microtektites (including 1 normal, 3 high-Ni, 1 high-Mg, and 1 intermediate sample) have been sampled from ODP Site 769A, and cores RC12-331 and RC14-46; Ivory Coast microtektites (10 samples) come from core K9-56; North American microtektites (25 samples) come from DSDP Sites 612, 94, and 149, core RC9-58, and from Bath Cliff, Barbados. The compositions of these samples have already been studied (Glass et al. 2004) and are reported in Table 1. The spherules have been embedded in resin, ground down to expose the interior surface, and polished. Typical dimensions range from 400 to 800 μm diameter. Both scanning electron microscopy and optical microscopy indicate that no crystals are present. As shown in Figure 1, most of the microtektite samples display silica contents ranging between ca. 70 and 80 wt% and alkali contents ranging between ca. 3 and 5 wt%.

The standards used for X-ray absorption near edge spectroscopy (XANES) measurements are: a staurolite from Canton Ticino (Switzerland) and a synthetic Fe-akermanite for Fe^{2+} in tetrahedral coordination; a grandidierite from Madagascar for Fe^{2+} in trigonal dipyramidal coordination; a synthetic kirschsteinite, a synthetic orthopyroxene ($En_{60}Fs_{40}$) and a siderite from Erzberg (Austria) for Fe^{2+} in octahedral coordination; an andradite from Italy, and an aegirine from Malawi for Fe^{3+} in octahedral coordination; a yoderite from Mautia Hills (Tanzania) for Fe^{3+} in fivefold coordination; a tetra-ferriphlogopite from Tapira (Brazil) for Fe^{3+} in fourfold coordination (Giuli et al. 2001). The natural standards were separated by hand-picking from centimeter-sized crystals choosing the clearest portions to avoid impurities. All the standards were checked for purity by both optical microscopy and X-ray diffraction. Model compounds for X-ray absorption spectroscopy (XAS) measurement were prepared by smearing finely ground powder

on a kapton tape, whereas the glass samples were prepared as slides with polished surfaces. Fe *K*-edge XANES spectra were recorded at room temperature at the ESRF (European Synchrotron Radiation Facility) storage ring on the undulator beamline ID26 (Gauthier et al. 1999; Solé et al. 1999) operating at 6 GeV. A Si(311) double-crystal monochromator was used, providing an energy resolution of ~0.2 eV at the Fe *K*-edge. However, the main limitation for energy resolution is the finite core-hole width of the absorbing element (~1.15 eV at the Fe *K*-edge, Krause and Oliver 1979), resulting in a convoluted energy resolution of ~1.4 eV. The energy was calibrated by defining the first derivative peak of a metallic Fe reference foil to be at 7112.0 eV. Two Si mirrors were used for the harmonics rejection of the incident X-ray beam. Beam dimension at the sample was 55 × 120 µm. For each sample the beam has been carefully centered by means of vertical and horizontal scans so as to allow probing the inner part of the spherules far from the border, thus avoiding possible alteration rims. XANES data were recorded in quick-scan mode by simultaneously scanning the monochromator angle and the undulator gap with a typical energy step of 0.1 eV and counting 44 ms per point. Each scan took 120 s and an average of 12 spectra was taken per sample. The spectra were acquired in fluorescence mode, using a Si photo-diode, and I_0 was monitored by measuring the fluorescence signal of a titanium foil using a Si photo-diode. The flat surface of the sample was positioned at 45° with respect to the beam and the detector. Average of about 12 scans for each sample allowed us to obtain very good signal to noise ratios despite the small beam size. The energy reproducibility has been estimated to be ±0.03 eV or better.

Experimental XANES spectra were reduced by background subtraction with a linear function and then normalized for atomic absorption on the average absorption coefficient of the spectral region from 7170 to 7350 eV. The threshold energy was taken as the first maximum of the first derivative of the spectra, whereas peak positions were obtained by calculating the second derivative of the spectra. Pre-edge peak analysis was carried out following the same procedure reported in Wilke et al. (2001) and Giuli et al. (2002). The pre-edge peak was fitted by a sum of pseudo-Voigt functions, and their intensities along with energy positions were compared with those of the standards analyzed here and others from the literature (e.g., Wilke et al. 2001; Farges 2001) to extract information on Fe oxidation state and coordination number in these microtektites. Particular care was taken in using the smallest possible number of components in the pre-edge peak fitting procedure. In particular, the number (and, in some cases, the approximate energy) of the components was constrained to equal the number (and approximate energy) of the minima in the second derivative spectrum of the pre-edge peak. Several different procedures have been attempted for peak fitting: simultaneous fitting of the background and the pseudo-Voigt component; preliminary background subtraction followed by fitting with pseudo-Voigt component allowing the components to have different full-width at half maximum (FWHM) or Lorentian character; preliminary background subtraction followed by fitting with pseudo-Voigt component constrained to have the same FWHM and Lorentian character. This last procedure has been shown to produce the best results in terms of data scatter.

The precision of the fitted pre-edge peak centroid energy and integrated area are ±0.02 eV and ±0.015, respectively. Mixing lines have been calculated as linear combination of two pre-edge peaks representative of Fe^{2+} and Fe^{3+} (see Giuli et al. 2003, 2011). We tried different integrated areas for Fe^{2+} and Fe^{3+} end-members until a calculated mixing line was found to match the integrated area and centroid energy of a set of glasses; then it has been used to evaluate the contribution of the divalent and trivalent Fe to the experimentally measured pre-edge peaks. This procedure implies that a single spectrum (pre-edge peak integrated area and centroid energy) does not allow an accurate determination of the $Fe^{3+}/(Fe^{2+}+Fe^{3+})$ ratio unless contrains are applied on the integrated areas relative to the Fe^{3+} and Fe^{2+} species contributing to that spectrum. This procedure, applied to a set of synthetic glasses (Giuli et al. 2011), resulted in accurate determinations of $Fe^{3+}/(Fe^{2+}+Fe^{3+})$ ratios that are in agreement with independent titration data within ±0.03. In the present case we estimate the error in the determination of $Fe^{3+}/(Fe^{2+}+Fe^{3+})$ ratios on microtektite samples to be ±0.05.

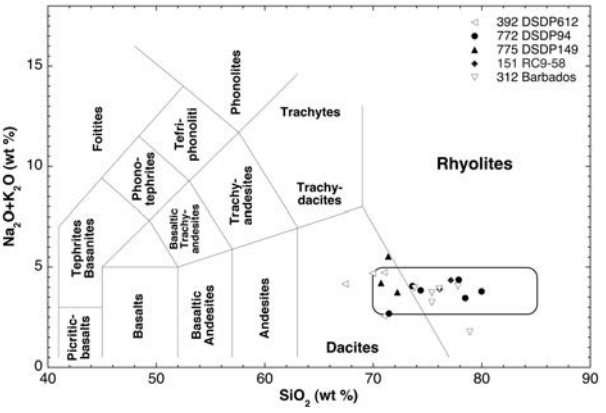

FIGURE 1. Total alkalis vs. silica contents of the analyzed North American microtektites. For source of compositional data see Table 1. The open rectangle represents the range in the silica and alkali contents for North American tektites as reported by Glass et al. (1995, 1998) and Montanari and Koeberl (2000). Each sample group was given the designation NA plus the sample name (three digit number) as reported in Glass et al. (2004) and the collection site.

XANES RESULTS

Examples of experimental Fe *K*-edge XANES spectra are shown in Figure 2 for five groups of microtektites: Australasian and Ivory Coast in Figures 2a and 2b, respectively, and three groups of North American microtektites in Figures 2c, 2d, and 2e. The shape and edge energy position of the Australasian and Ivory Coast microtektite spectra are very similar to those of splash form tektites studied previously (Giuli et al. 2002), suggesting the presence of predominantly divalent Fe. On the other hand, the spectra of the North American microtektite samples display significant differences in both the shape of the XANES spectra and their first derivative that are clearly related to variations in the Fe oxidation state. Moreover, also significant changes in the pre-edge peak (labeled P) are visible.

The pre-edge peak is related to an *s-d* like electronic transition and, despite being dipole-forbidden, can become partially allowed by mixing of the *d*-states of the transition metal with the *p*-states of the surrounding oxygen atoms. This means that the pre-edge peak energy position and intensity depend strongly on both the geometry around Fe and on the mean Fe oxidation state (Calas and Petiau 1983; Brown et al. 1995). As already shown in the literature, accurate evaluation of the pre-edge peak centroid energy and integrated area and comparison with those of Fe model compounds can provide quantitative information on both Fe oxidation state and coordination environment (see Calas and Petiau 1983; Brown et al. 1995; Wilke et al. 2001, 2006; Farges 2001; Giuli et al. 2002, 2011): its intensity will be almost zero in case of regular octahedral symmetry (O_h) around the absorber, whereas it will reach its maximum in the case of tetrahedral simmetry (T_d).

The background subtracted pre-edge peaks of the microtektite XANES spectra are shown in Figures 3a–3e), along with the pseudo-Voigt components used in the fitting procedure and their sums, whereas their centroid energies and integrated areas are reported in Table 2. Each pre-edge peak can be fitted with two to three components whose energies (ca. 7112.6, 7113.9–7114.3, and 7114.5–7115.3 eV) are consistent with those of divalent and trivalent Fe model compounds. In particular, while the first and last components can be ascribed to contributions from Fe^{2+} and Fe^{3+}, respectively, the component at intermediate energy results from contributions by both Fe^{2+} and Fe^{3+}. The relative importance of divalent or trivalent Fe causes an increase of the respective components resulting in an energy shift of the pre-edge peak centroid.

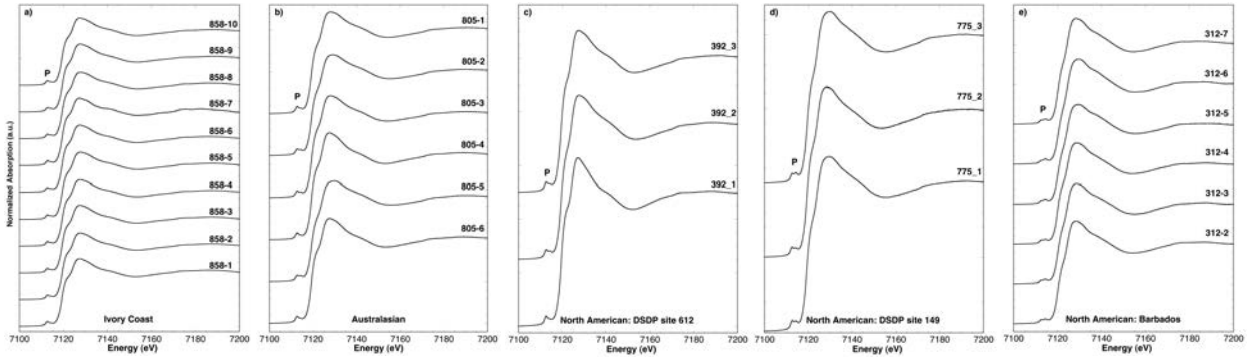

FIGURE 2. Experimental Fe *K*-edge XANES spectra of microtektites: (**a**) Ivory Coast; (**b**) Australasian; (**c**) North American (DSDP 612); (**d**) North American (DSDP 149); (**e**) North American (Barbados). Pre-edge peak is labeled "P". The spectra labels are the same as sample names in Table 1. The first three digits refers to the disk number the microtektites were mounted on and the number after the hyphen refers to the number of the microtektite on that disk.

The integrated area of the pre-edge peaks vs. their centroid energies are plotted in Figures 4a and 4b) along with the data of Fe model compounds analyzed here and by others (Wilke et al. 2001; Farges 2001; Giuli et al. 2002). For the sake of simplicity, the relative energy is plotted (0 refers to the first maximum of the first derivative of metallic Fe spectrum) to avoid confusion when comparing with literature data where a different energy value of metallic Fe has been chosen. All divalent Fe model compounds plot at energies close to 0.9 eV above the metallic Fe edge, whereas trivalent Fe model compounds plot at energies close to 2.4 eV. At constant energy, the intensity of the model compounds pre-edge peaks varies according to the Fe coordination geometry (the shaded ellipses refer to the range of coordination numbers in Fe model compounds).

The Australasian and Ivory Coast microtektites data (Fig. 4a) plot within a narrow region close in energy to that of divalent Fe model compounds, meaning that most of the Fe is divalent. Three mixing lines (dotted line with small diamonds) have been calculated by a linear combination of (1) a pre-edge peak with a centroid at 0.9 eV above the edge of metallic iron and an integrated area intermediate to that of $^{[4]}Fe^{2+}$ and $^{[5]}Fe^{2+}$ model compounds and (2) a pre-edge peak with a centroid at 2.4 eV above the edge of metallic iron and integrated area typical of $^{[4]}Fe^{3+}$, $^{[5]}Fe^{3+}$, or $^{[6]}Fe^{3+}$.

These mixing lines stem from a region with intermediate intensity between $^{[4]}Fe^{2+}$ and $^{[5]}Fe^{2+}$ thus meaning that the divalent Fe in these glasses is present both in fourfold- and fivefold-coordination. Should $^{[6]}Fe^{2+}$ be present in consistent amounts it would drastically lower the pre-edge peak intensity. However, its presence in minor amounts cannot be ruled out by XANES data alone. The two mixing lines that best fit the experimental points are those calculated using $^{[4]}Fe^{3+}$ and $^{[5]}Fe^{3+}$ pre-edge peak intensity; this suggests that trivalent iron may be in fourfold- and fivefold-coordination.

Comparison between the experimental pre-edge peak data and the calculated mixing lines provided quantitative $Fe^{3+}/(Fe^{3+}+Fe^{2+})$ ratios $\leq 0.1 \pm 0.05$ for most of the samples and up to 0.21 for four samples (0.13, 0.15, 0.19, and 0.21). Based on the precision of the energy (±0.03 and ±0.05 eV for the Ivory Coast and Australasian spectra, respectively), we estimate the error in the $Fe^{3+}/(Fe^{3+}+Fe^{2+})$ ratios to be within ±0.05. These results are in keeping with known Fe oxidation states of Australasian and Ivory Coast microtektites.

On the other hand, North American microtektites display centroid energy values much higher than those of the Australasian and Ivory Coast microtektites, indicating significantly higher contributions from trivalent Fe (Fig. 4b). Three mixing lines have been calculated as in the previous case. It is worth remarking that this set of mixing lines originates from a point with the average intensity of a wide set of tektites analyzed so far (Giuli et al. 2002, 2010a, 2010b). As in the Ivory Coast and Australasian microtektite case, the average coordination number of divalent

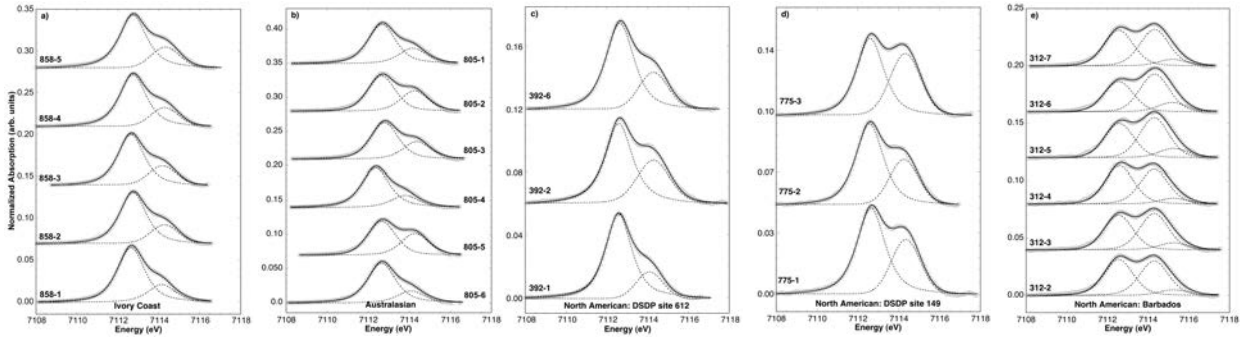

FIGURE 3. Background subtracted pre-edge peaks: (**a**) Ivory Coast; (**b**) Australasian; (**c**) North American (DSDP Site 612); (**d**) North American (DSDP Site 149); (**e**) North American (Barbados). Labels as in Figure 2.

TABLE 2. Pre-edge peak features in the samples studied

Sample name	Centroid (eV)*	Integrated intensity	Fit agreement index (%)	$Fe^{3+}/(Fe^{2+}+Fe^{3+})$
Ivory Coast microtektites				
858-1	7112.98	0.149	99.97	0.03
858-2	7113.15	0.142	99.95	0.17
858-3	7113.08	0.141	99.96	0.12
858-4	7113.15	0.146	99.97	0.15
858-5	7113.21	0.157	99.97	0.12
858-6	7113.13	0.160	99.97	0.08
858-7	7113.16	0.161	99.97	0.09
858-8	7113.24	0.163	99.96	0.13
858-9	7113.22	0.155	99.97	0.15
858-10	7113.08	0.152	99.97	0.06
Australasian microtektites				
805-1	7112.93	0.141	99.92	0.02
805-2	7113.28	0.143	99.98	0.22
805-3	7112.98	0.137	99.96	0.04
805-4	7113.13	0.139	99.95	0.13
805-5	7113.23	0.144	99.92	0.19
805-6	7113.03	0.143	99.92	0.07
North American microtektites				
392-1	7112.94	0.130	99.98	0.02
392-2	7113.18	0.146	99.94	0.16
392-6	7113.12	0.149	99.95	0.12
775-1	7113.33	0.149	99.87	0.26
775-2	7113.19	0.136	99.94	0.24
775-3	7113.40	0.151	99.94	0.30
312-2	7113.56	0.128	99.87	0.50
312-3	7113.61	0.123	99.90	0.54
312-4	7113.53	0.124	99.89	0.50
312-5	7113.71	0.131	99.91	0.61
312-6	7113.72	0.123	99.92	0.58
312-7	7113.58	0.127	99.92	0.52
772-1	7113.24	0.138	99.96	0.25
772-2	7113.38	0.138	99.86	0.35
772-3	7113.15	0.170	99.94	0.06
772-4	7113.52	0.143	99.87	0.42
772-5	7113.12	0.161	99.92	0.06
772-6	7113.14	0.131	99.94	0.22
772-7	7113.57	0.133	99.85	0.49
151-91a	7113.48	0.152	99.93	0.35
151-93a	7113.54	0.161	99.95	0.36
151-93b	7113.29	0.135	99.95	0.30
151-94a	7113.45	0.130	99.93	0.43
151-101b	7113.55	0.135	99.92	0.47
151-102a	7113.37	0.148	99.96	0.29

* The energy has been calibrated by setting the edge energy of metallic Fe at 7112.0 eV.

Fe is intermediate between [4] and [5]. However, while many the samples can be explained as consisting of a mixture of $^{[4]}Fe^{2+}$, $^{[5]}Fe^{2+}$, $^{[4]}Fe^{3+}$, and $^{[5]}Fe^{3+}$ (see Calas et al. 1983; Brown et al. 1995; Rossano et al. 1999; Wilke et al. 2004, 2006; Jackson et al. 2005; Giuli et al. 2002, 2011; Weigel et al. 2006, 2008), which are common Fe species usually found in silicate melts and glasses, the microtektites from Barbados have distinctly lower integrated areas, compatible with the presence of $^{[6]}Fe^{3+}$ along with other Fe species. Despite this Fe species not being very common in silicate melts and glasses, it has been observed by Wilke et al. (2004) in synthetic glasses of basaltic composition. Comparison between the experimental pre-edge peak data of NA microtektites and the calculated mixing lines provided quantitative $Fe^{3+}/(Fe^{3+}+Fe^{2+})$ ratios ranging from 0.02 and 0.61 ± 0.05.

DISCUSSION

XANES data have been presented for a large set of microtektites from the Australasian, Ivory Coast, and North American strewn fields (6, 10, and 26 samples, respectively). Accurate analysis of the pre-edge peak allowed determination of the Fe oxidation state for all the samples analyzed (see Table 2). To the authors' knowledge, this is the first report of the Fe oxidation state in such a large set of microtektites.

Most of the samples from the Australasian and Ivory Coast strewn fields display values consistent with $Fe^{3+}/(Fe^{2+}+Fe^{3+})$ ratios $\leq 0.1 \pm 0.05$, with only four samples displaying slightly larger values (0.13, 0.15, 0.19, and 0.21). Thus, in these two strewn fields, microtektites display Fe oxidation states and coordination numbers fairly similar to those of macroscopic tektites (Fudali et al. 1987; Dunlap et al. 1998; Rossano et al. 1999; Giuli et al. 2002, 2010a, 2010b). On the other hand, microtektites from the North American strewn field exhibit much higher values of the $Fe^{3+}/(Fe^{2+}+Fe^{3+})$ ratios, from 0.02 up to 0.61 ± 0.05.

As there is the possibility that a long residence time in marine sediments may have altered the microtektite glasses, we checked whether some correlation may exist between Fe oxidation state and chemical composition, which may be indicative of sea-water

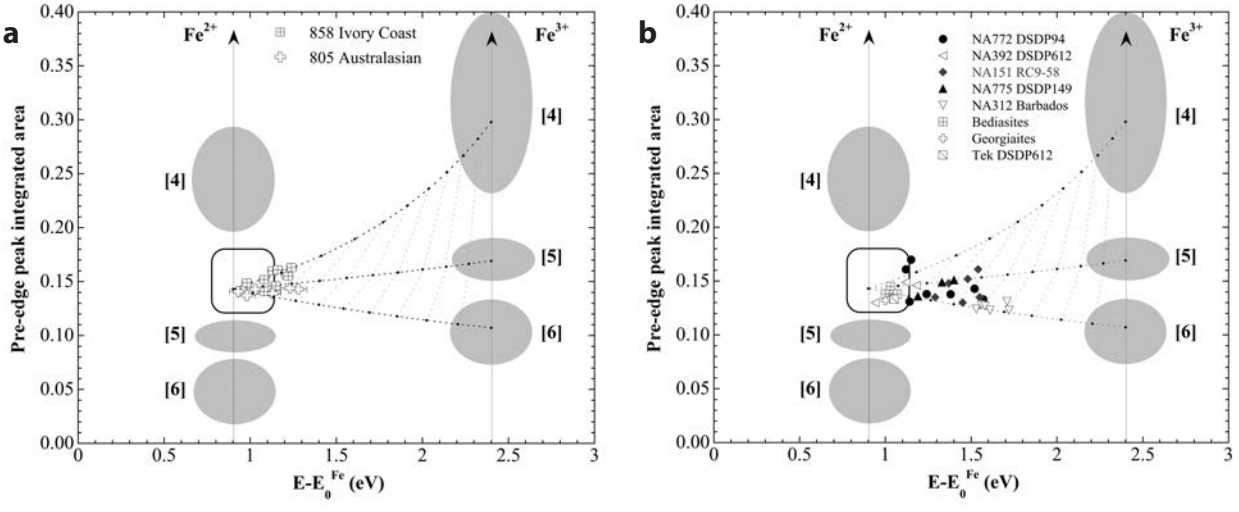

FIGURE 4. Pre-edge peak integrated area vs. centroid energy of: (**a**) Ivory Coast and Australasian microtektites; (**b**) North American microtektites. Symbols as in Figure 1. The 0 on the x axis refers to the edge energy of metallic iron (7112.0 eV).

alteration induced oxidation (see Giorgetti et al. 2001; Alt and Mata 2000). In Figure 5 the alkali content is plotted as a function of the $Fe^{3+}/(Fe^{2+}+Fe^{3+})$ ratio of all the microtektites analyzed here. No obvious correlation has been found between Fe oxidation state and chemical composition of the studied microtektites. In particular, no inverse relationship has been found with the Na content, which might have been expected in case of oxidation due to seawater alteration, nor any other correlation has been found that would suggest alteration in a marine environment. Moreover, a tektite fragment retrieved along with microtektites from a core in the DSDP Site 612 (and which, thus, should have similar degree of alteration) displayed an $Fe^{3+}/(Fe^{2+}+Fe^{3+})$ ratio of 0.05 ± 0.05, consistent with values for the tektites found on land (Giuli et al. 2010a), thus further suggesting that there was no alteration-induced oxidation in these microtektite samples. Also preliminary micro-infrared spectroscopy data on a few microtektite samples (see supplementary material[1]) yielded low water contents in the range between 35 to 455 ppm, similar to those of NA tektites [see Beran and Koeberl 1997; Giuli et al. 2010c (IMA abstract)], reinforcing the suggestion that the microtektites analyzed here did not suffer alteration.

Thus, we believe that the oxidation states determined are a signature of the formation process of these NA microtektites, and not the product of subsequent alteration in the sediment. Interestingly, pre-edge data of all NA microtektites seem to define different trends all originating from a single narrow region whose energy and intensity is typical of most splash form tektites studied so far. Also, previous data on NA tektites (Giuli et al. 2010a) from different locations and with different chemistry clearly show that the Fe oxidation state of tektites does not vary sensibly according to tektite composition. This indicates that the wide range of Fe oxidation states we found in NA microtektites is not related to lateral heterogeneity of the target rock.

A possible explanation may involve formation of microtektites with Fe oxidation state and coordination number similar to that of tektites and Trinity glass (a glass formed by high-temperature melting of desert sand during the first atomic bomb test at the Trinity site; see Glass et al. 1988; Giuli et al. 2010b) and subsequent oxidation when still molten.

Although a similarity with impact glass spherules from the K/T boundary, which showed a similar trend in pre-edge peak data extending up to 100% trivalent Fe, may be envisioned (Giuli et al. 2005, 2008a), no clear explanation can be provided yet for the high-Fe oxidation state of the North American microtektites.

In this respect, it is interesting to notice that the Fe oxidation state of the studied microtektites seems to increase with the distance of the collection site from the source crater. In Figure 6 the fraction of the trivalent Fe is shown as a function of the distance of the microtektite collection site from the Chesapeake Bay impact structure: even though microtektites within every collection site display a range of Fe oxidation states, it is evident that the fraction of trivalent Fe tends to increase with the distance from the crater. Although it would be tempting to relate the increase of the trivalent Fe fraction to the oxidation of melt in air during the travel from the source crater to the landing site, this hypothesis has to be discounted when comparing data for Australasian microtektites with those found in Antarctica (Folco et al. 2010). In fact, recent analyses of the Fe oxidation state on 29 Antarctic microtektite samples (Giuli et al. 2012) showed that the fraction of trivalent Fe is lower than 0.1, thus being compatible with the Fe oxidation state of Australasian

[1] Deposit item AM-13-1111, Supplemental Information. Deposit items are stored on the MSA web site and available via the *American Mineralogist* Table of Contents. Find the article in the table of contents at GSW (ammin.geoscienceworld.org) or MSA (www.minsocam.org), and then click on the deposit link.

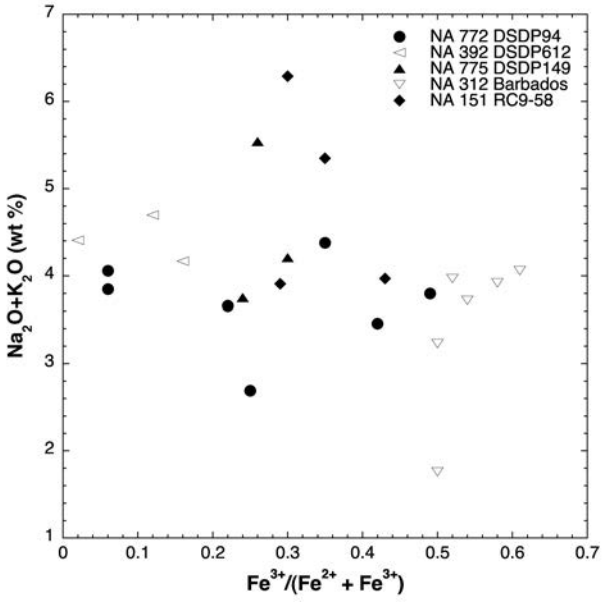

FIGURE 5. Alkali content (oxide wt%) as a function of the fraction of trivalent Fe in the studied microtektites. The amount of both Na_2O and K_2O does not show any significant decrease as would be expected in case of sea water alteration.

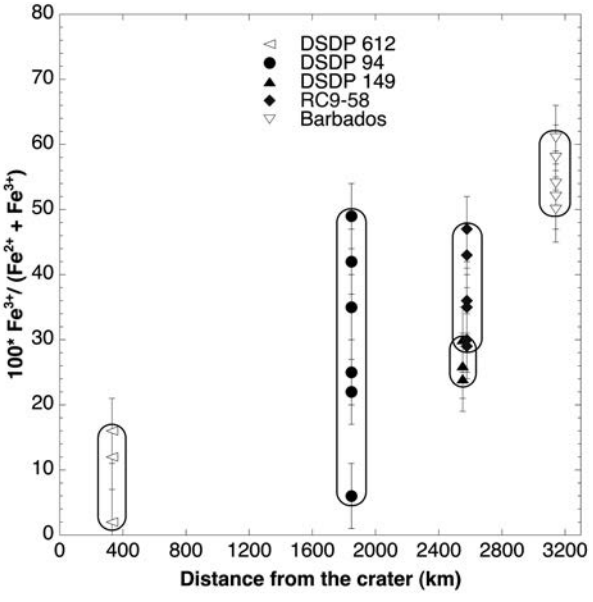

FIGURE 6. Trivalent Fe fraction of the NA microtektites as a function of collection site distance from the source crater (symbols as in Fig. 4b). A marked increase of the trivalent Fe at increasing distance from the crater is evident.

tektites previously analyzed (see Dunlap et al. 1998; Dunlap and Sibley 2004; Rossano et al. 1999; Giuli et al. 2002) and the microtektites analyzed here. In that case, a flight distance of up to ca. 11 000 km from the putative location of the source crater did not produce any noticeable oxidation of the Fe in the microtektite melt droplet; thus, oxidation in air during the flight is unlikely to be responsible for the higher Fe oxidation state of NA microtektites compared to tektites.

IMPLICATIONS

Even though the Fe oxidation in North American microtektites could be explained by interaction of melt droplets with a H_2O-rich vapor plumes generated during the impact, no definitive explanation can yet be given for the anomalously high-Fe oxidation state of NA microtektites and more studies are needed to understand the factors affecting the Fe oxidation state of these samples. However, the marked difference in the $Fe^{3+}/(Fe^{2+}+Fe^{3+})$ ratio of tektites and microtektites from the North American strewn field raises the question whether or not microtektites should simply be considered as microscopic analogous of tektites or if some difference exists between their formation mechanisms. Furthermore, our results indicate that some differences must exist in the thermal (and/or oxygen fugacity) histories of microtektites from the NA strewn field compared with those from the Ivory Coast or the Australasian strewn fields.

ACKNOWLEDGMENTS

We thank the staff of beamline ID-26 (ESRF, France) for kind assistance during the experiment. Helpful comments by the reviewers are also greatly appreciated.

REFERENCES CITED

Alt, C.J., and Mata, B.P. (2000) On the role of microbes in the alteration of submarine basaltic glass: a TEM study. Earth and Planetary Science Letters, 181, 301–313.

Beran, A., and Koeberl, C. (1997) Water in tektites and impact glasses by Fourier-transformed infrared spectrometry. Meteoritics & Planetary Science, 32, 211–216.

Brown, G.E., Farges, F., and Calas, G. (1995) X-ray scattering and X-ray spectroscopy studies of silicate melts. In J.F. Stebbins, P.F. McMillan, D.B. Dingwell, Eds., Structure, dynamics and properties of silicate melts, vol. 32, p. 317–410. Review in Mineralogy, Mineralogical Society of America, Chantilly, Virginia.

Burns, C.A. (1985) A study of North American microtektites from Barbados, West Indies: M.S. Thesis, 120 pp. University of Delaware, Newark.

Calas, G., and Petiau, J. (1983) Coordination of iron in oxide glasses through high-resolution K-edge spectra: information from the pre-edge. Solid State Communications, 48, 625–629.

Cassidy, W.A., Glass, B.P., and Heezen, B.C. (1969) Physical and chemical properties of Australasian microtektites. Journal of Geophysical Research, 74, 1008–1025.

Dunlap, R.A., and Sibley, A.D.E. (2004) A Mössbauer effect study of Fe site occupancies in Australasian tektites. Journal of Non-Crystalline Solids, 337, 36–41.

Dunlap, R.A., Eelman, D.A., and MacKay, G.R. (1998) A Mössbauer effect investigation of correlated hyperfine parameters in natural glasses (tektites). Journal of Non-Crystalline Solids, 223, 141–146.

Farges, F. (2001) Crystal-chemistry of Fe in natural grandidierites: a XAFS spectroscopy study at the Fe K-edge. Physics and Chemistry of Minerals, 28, 619–629.

Folco, L., Glass, B.P., D'Orazio, M., and Rochette, P. (2010) A common volatilization trend in Transantarctic Mountain and Australasian microtektites: Implications for their formation model and parent crater location. Earth and Planetary Science Letters, 293, 135–139.

Fudali, R.F., Dyar, M.D., Griscom, D.L., and Schreiber, D. (1987) The oxidation state of iron in tektite glass. Geochimica et Cosmochimica Acta, 51, 2749–2756.

Gauthier, C., Solé, V.A., Signorato, R., Goulon, J., and Moguiline, E. (1999) The ESRF beamline ID26: X-ray absorption on ultra dilute sample. Journal of Synchrotron Radiation, 6, 164–166.

Giorgetti, G., Marescotti, P., Cabella, R., and Lucchetti, G. (2001) Clay mineral mixtures as alteration products in pillow basalts from the eastern flank of Juan de Fuca Ridge: a TEM-AEM study. Clay Minerals, 36, 75–91.

Giuli, G., Paris, E., Wu, Z., Brigatti, M.F., Cibin, G,. Mottana, A., and Marcelli, A. (2001) Experimental and theoretical XANES and EXAFS study of tetraferriphlogopite. European Journal of Mineralogy, 13, 1099–1108.

Giuli, G., Pratesi, G., Cipriani, C., and Paris, E. (2002) Fe local structure in tektites by extended X-ray Absorption fine structure and high resolution X-ray absorption near edge spectroscopy. Geochimica et Cosmochimica Acta, 66, 4347–4353.

Giuli, G., Paris, E., Pratesi, G., Koeberl, C., and Cipriani, C. (2003) Iron oxidation state in the Fe-rich layer and silica matrix of Libyan Desert Glass: a high resolution XANES study. Meteoritics & Planetary Science, 38, 1181–1186.

Giuli, G., Eeckhout, S.G., Paris, E., Koeberl, C., and Pratesi, G. (2005) Iron oxidation state in impact glass from the K/T boundary at Beloc, Haiti, by high-resolution XANES spectroscopy. Meteoritics & Planetary Science, 40, 1575–1580.

Giuli, G., Eeckhout, S.G., Koeberl, C., Pratesi, G., and Paris, E. (2008a) Yellow impact glass from the K/T boundary at Beloc (Haiti): XANES determination of the Fe oxidation state and implications for formation conditions. Meteoritics & Planetary Science, 43, 981–986.

Giuli, G., Eeckhout, S.G., Cicconi, M.R., Koeberl, C., Glass, B.P., Pratesi, G., and Paris, E. (2008b) North American microtektites are more oxidized compared to tektites. Large Meteorite Impacts and Planetary Evolution IV, Johannesburg, Lunar and Planetary Institute 1423, p. 88–89 (abstract).

Giuli, G., Eeckhout, S.G., Cicconi, M.R., Koeberl, C., Pratesi, G., and Paris, E. (2010a) Iron oxidation state and local structure in North American tektites. In W.U. Reimold and R. Gibson, Eds., Large Meteorite Impacts and Planetary Evolution IV, 465, p. 645–652. Geological Society of America Special Paper.

Giuli, G., Pratesi, G., Eeckhout, S.G., Koeberl, C., and Paris, E. (2010b) Iron reduction in silicate glass produced during the 1945 nuclear test at the trinity site (Alamogordo, New Mexico, USA). In W.U. Reimold and R. Gibson, Eds., Large Meteorite Impacts and Planetary Evolution IV, 465, p. 653–662. Geological Society of America Special Paper.

Giuli, G., Eeckhout, S.G., Cicconi, M.R., Koeberl, C., Glass, B.P., Pratesi, G., Cestelli-Guidi M., Marcelli A., Carroll, M.R., and Paris, E. (2010c) Tektites and microtektites Fe oxidation state and water content. Proceedings of the 20th General Meeting of the International Mineralogical Association. 21–27 August 2010, Budapest. Acta Mineralogica Petrografica, 6, 777 (abstract).

Giuli, G., Paris, E., Hess, K.U., Dingwell, D.B., Cicconi, M.R., Eeckhout, S.G., Fehr, K.T., and Valenti, P. (2011) XAS determination of the Fe local environment and oxidation state in phonolite glasses. American Mineralogist, 96, 631–636.

Giuli, G., Cicconi, M.R., Eeckhout, S.G., Paris, E., Pratesi, G., and Folco, L. (2012) Fe Oxidation State in Microtektites from the Transantarctic Mountains. 43rd Lunar and Planetary Science Conference, March 19–23, The Woodlands, Texas. LPI Contribution No. 1659, id. 1927.

Glass, B.P. (1967) Microtektites in deep-sea sediments. Nature, 214, 372–374.

——— (1968) Glassy objects (microtektites?) from deep-sea sediments near the Ivory Coast. Science New Series, 161, 3844, 891–893.

——— (1972) Australasian microtektites in deep-sea sediments. In D.E. Hayes, Ed., Antarctic Oceanology II: The Australian-New Zealand Sector, Antarctic Research Series, 19, p. 335–348. American Geophysical Union, Washington, D.C.

——— (1989) North American tektite debris and impact ejecta from DSDP Site 612. Meteoritics, 24, 209–218.

——— (1990) Tektites and microtektites: key facts and inferences. Tectonophysics, 171, 393–404.

Glass, B.P., and Pizzuto, J.E. (1994) Geographic variation in Australasian microtektite concentrations: Implications concerning the location and size of the source crater. Journal of Geophysical Research, 99, 9, 19075–19081.

Glass, B.P., Senfltle, F.E., Muenow, D.W., Aggrey, K.E., and Thorpe, A.N. (1988) Atomic bomb glass beads: tektite and microtektite analogs. In Proceedings, Second International Conference on Natural Glasses, Prague, September, 1987, 361–369.

Glass, B.P., Koeberl, C., Blum, J.D., Senftle, J., Izett, G.A., Evans, B.J., Thorpe, A.N., Povenmire, H., and Strange, R.L. (1995) A Muong Nong–type Georgia tektite. Geochimica et Cosmochimica Acta, 59, 4071–4082.

Glass, B.P., Koeberl, C., Blum, J.D., and McHugh, C.M.G. (1998) Upper Eocene tektite and impact ejecta layer on the continental slope off New Jersey. Meteoritics & Planetary Science, 33, 229–241.

Glass, B.P., Huber, H., and Koeberl, C. (2004) Geochemistry of Cenozoic microtektites and clinopyroxene-bearing spherules. Geochimica et Cosmochimica Acta, 68, 3971–4006.

Jackson, W.E., Farges, F., Yeager, M., Mabrouk, P.A., Rossano, S., Waychunas, G.A., Solomon, E.I., and Brown, G.E. Jr. (2005) Multispectroscopic study of Fe(II) in silicate glasses: Implications for the coordination environment of Fe(II) in silicate melts. Geochimica et Cosmochimica Acta, 69, 4315–4332.

Koeberl, C. (1986) Geochemistry of tektites and impact glasses: Annual Reviews of Earth and Planetary Science, 14, 323–350.

——— (1994) Tektite origin by hypervelocity asteroidal or cometary impact: Target rocks, source craters, and mechanisms. In B.O. Dressler, R.A.F. Grieve, and V.L. Sharpton, Eds., Large Meteorite Impacts and Planetary Evolution, 293, p. 133–152. Geological Society of America Special Paper.

Krause, M.O., and Oliver, J.H. (1979) Natural widths of atomic K and L levels, K alpha

X-ray lines and several KLL auger lines. Journal of Physical and Chemical Reference Data, 8, 329–338.
Montanari, A., and Koeberl C. (2000) Impact stratigraphy. Lecture Notes in Earth Sciences, 93, 364 p. Springer Verlag, Heidelberg-Berlin.
Rossano, S., Balan, E., Morin, G., Bauer, J.P., Calas, G., and Brouder, C. (1999) ^{57}Fe Mössbauer spectroscopy of tektites. Physics and Chemistry of Minerals, 26, 530–538.
Senftle, F.E., Thorpe, A.N., and Sullivan, S. (1969) Magnetic properties of microtektites. Journal of Geophysical Research, 74, 6825–6833.
Solé, A.V., Gauthier, C., Goulon, J., and Natali, F. (1999) Undulator QEXAFS at the ESRF beamline ID26. Journal of Synchrotron Radiation, 6, 174–175.
Weigel, C., Cormier, L., Galoisy, L., Calas, G., Bowron, D., and Beuneu, B. (2006) Determination of Fe^{3+} sites in a $NaFeSi_2O_6$ glass by neutron diffraction with isotopic substitution coupled with numerical simulation. Applied Physics Letters, 89, 141911.
Weigel, C., Cormier, L., Calas, G., Galoisy, L., and Bowron, D.T. (2008) Nature and distribution of iron sites in a sodium silicate glass investigated by neutron diffraction and EPSR simulation. Journal of Non-Crystalline Solids, 354, 5378–5385.
Wilke, M., Farges, F., Petit, P.E., Brown, G.E., and Martin, F. (2001) Oxidation state and coordination of Fe in minerals: an Fe K-XANES spectroscopic study. American Mineralogist, 86, 714–730.
Wilke, M., Partzsch, G.M., Bernhardt, R., and Lattard, D. (2004) Determination of the iron oxidation state in basaltic glasses using XANES at the K-edge. Chemical Geology, 213, 71–87.
Wilke, M., Schmidt, C., Farges, F., Malavergne, V., Gautron, L., Simionovici, A., Hahn, M., and Petit, P-E. (2006) Structural environment of iron in hydrous aluminosilicate glass and melt-evidence from X-ray absorption spectroscopy. Chemical Geology, 229, 144–161.

Manuscript received February 15, 2013
Manuscript accepted July 24, 2013
Manuscript handled by Daniel Neuville